

Searching for $z \sim 7.7$ Ly α Emitters in the COSMOS Field with NEWFIRM

Hannah B. Krug¹, Sylvain Veilleux¹, Vithal Tilvi^{2,3}, Sangeeta Malhotra², James Rhoads², Pascale Hibon^{2,4}, Rob Swaters⁴, Ron Probst⁵, Arjun Dey⁵, Mark Dickinson⁵, & Buell T. Jannuzi⁵

ABSTRACT

The study of Ly α emission in the high-redshift universe is a useful probe of the epoch of reionization, as the Ly α line should be attenuated by the intergalactic medium (IGM) at low to moderate neutral hydrogen fractions. Here we present the results of a deep and wide imaging search for Ly α emitters in the COSMOS field. We have used two ultra-narrowband filters (filter width of ~ 8 – 9 Å) on the NEWFIRM camera, installed on the Mayall 4m telescope at Kitt Peak National Observatory, in order to isolate Ly α emitters at $z = 7.7$; such ultra-narrowband imaging searches have proved to be excellent at detecting Ly α emitters. We found 5σ detections of four candidate Ly α emitters in a survey volume of 2.8×10^4 Mpc³ (total survey area ~ 760 arcmin²). Each candidate has a line flux greater than 8×10^{-18} erg s⁻¹ cm⁻². Using these results to construct a luminosity function and comparing to previously established Ly α luminosity functions at $z = 5.7$ and $z = 6.5$, we find no conclusive evidence for evolution of the luminosity function between $z = 5.7$ and $z = 7.7$. Statistical Monte Carlo simulations suggest that half of these candidates are real $z = 7.7$ targets, and spectroscopic followup will be required to verify the redshift of these candidates. However, our results are consistent with no strong evolution in the neutral hydrogen fraction of the IGM between $z = 5.7$ and $z = 7.7$, even if only one or two of the $z = 7.7$ candidates are spectroscopically confirmed.

Subject headings: dark ages, reionization — galaxies: high-redshift — galaxies: luminosity function

¹Department of Astronomy, University of Maryland, College Park, MD 20742, USA; E-mail: hkrug@astro.umd.edu, veilleux@astro.umd.edu

²School of Earth and Space Exploration, Arizona State University, Tempe, AZ 85287, USA

³Department of Physics & Astronomy, Texas A&M University, College Station, TX 77843, USA

⁴Gemini Observatory, La Serena, Chile

⁵NOAO, Tucson, AZ 85719, USA

1. INTRODUCTION

Direct observations of distant galaxies remain the most straightforward way to probe the fundamental nature of the high-redshift universe. Such observations can provide some much-needed constraints on numerical simulations, which may provide better answers to the question of how large scale structure forms and how star formation begins in dark matter halos. Star formation in early galaxies is dependent upon the mechanism by which gas cools; that mechanism itself is dependent upon the ionization state and metal enrichment of that gas which are not well constrained at high redshift. The Ly α emission line is a very useful tool for the detection of high-redshift galaxies, as the earliest stars in the universe should ionize surrounding hydrogen gas, which will then recombine to produce Ly α emission (see Willis et al. 2008). This Ly α line can be probed quite effectively at high redshifts via the use of narrowband filters, which focus on regions with low sky background and that are free of strong OH lines (e.g., Cuby et al. 2007). High-redshift objects should have essentially no flux blueward of rest-frame Ly α and none blueward of rest-frame 912 Å; this is a result of the Ly α forest effect at high redshift, due to strong absorption by intervening clouds (e.g., Bahcall & Salpeter 1965; Gunn & Peterson 1965; Lynds 1971; Rees 1986; Miralda-Escudé et al. 1996; Schaye 2001). Such narrowband surveys have proved quite successful so far (e.g., Cowie & Hu 1998; Hu et al. 1999; Rhoads et al. 2000; Fynbo et al. 2001; Ouchi et al. 2001; Hu et al. 2002; Malhotra & Rhoads 2002; Ouchi et al. 2003; Rhoads et al. 2003; Hu et al. 2004; Malhotra & Rhoads 2004; Rhoads et al. 2004; Taniguchi et al. 2005; Kashikawa et al. 2006; Shimasaku et al. 2006; Nilsson et al. 2007; Ouchi et al. 2008; Finkelstein et al. 2009) and have resulted in samples of galaxies over a range of redshifts, including the spectroscopic confirmation of a Ly α emitting galaxy at $z = 6.96$ (Iye et al. 2006). Even when these narrowband surveys do not successfully detect high- z objects, such null results can be used to constrain the Ly α luminosity function (e.g., Cuby et al. 2007; Willis et al. 2008; Sobral et al. 2009).

The early universe is expected to be metal poor, but metals have been detected in the intergalactic medium (IGM) at $z = 5.7$ (Ryan-Weber et al. 2006), and so the IGM must have been enriched in metals by $z \sim 6$ at the latest, with recent results tentatively indicating a metallicity downturn between $z \sim 5.7$ and $z \sim 5$ (Simcoe et al. 2011). Additionally, the Ly α line is sensitive to IGM obscuration at neutral hydrogen fractions ranging from low to high (e.g., $10\% \lesssim x_{HI} < 100\%$; Haiman 2002; Santos 2004), and thus observations of Ly α -emitting galaxies serve as a powerful probe of the reionization history of the universe; the Gunn-Peterson test, for example, is only useful when the neutral gas fraction is $< 1\%$ (Cuby et al. 2007). Increasing the neutral hydrogen fraction in the IGM increases the attenuation of Ly α emission from those galaxies (Sobral et al. 2009). As this neutral fraction increases, the Ly α luminosity function will vary according to the amount of light being at-

tenuated by the IGM. Previous estimates of the redshift of the epoch of reionization using constraints from studies of Ly α emitters do not concur with constraints derived from polarization observations of the CMB. The latter suggests that the redshift of reionization is $z_{\text{re}} = 10.5 \pm 1.2$, should reionization be an instantaneous process (Komatsu et al. 2011), whereas the former have indicated a significantly later end to the epoch. Constraints on the Ly α luminosity function (LF) can assist in determination of the redshift at which reionization has been completed, owing to the resonant scattering of Ly α photons in a neutral IGM. If the intrinsic number density of young galaxies remains constant over redshift, then a significant decline in the observed Ly α LF at a given redshift could indicate a change in IGM phase. On the lower redshift end, Malhotra & Rhoads (2004) found no significant evolution of Ly α LF between $5.7 < z < 6.6$; whereas at higher redshifts, an evolution of Ly α LF between $6.5 < z < 7$ is suggested based on single detections (Iye et al. 2006; Ota et al. 2008). Ouchi et al. (2008) found little evolution between $z \sim 3$ and $z \sim 6$ in the observed LFs, although they suggest a real evolution, with increase in intrinsic Ly α luminosity being canceled out by increase in IGM absorption. Curtis-Lake et al. (2011) have recently identified Ly α emitters at a high rate over $6 < z < 6.5$ in UKIDSS. Ono et al. (2011) have measured a decrease in Ly α emission line detection fraction over $6 < z < 7$, as have Schenker et al. (2011) over $6 < z < 8$ and Pentericci et al. (2011; following up work by Fontana et al. (2010)) over $6 < z < 7$; these studies are UV-continuum-selected galaxies (i.e., Lyman break galaxies) rather than selected via Ly α emission line but share the same goal, and all conclude that the neutral hydrogen fraction of the IGM is increasing over those epochs. The seven Ly α candidates found by Hibon et al. (2010) at $z = 7.7$ would indicate no evolution of the Ly α LF if they are found to be spectroscopically confirmed (although soon to be published work suggests that at least five are not confirmed; see Clément et al. (2011)); the four Ly α candidates found by Tilvi et al. (2010) could either indicate mild or no evolution between $6.5 < z < 7.7$ depending on the number of candidates which are confirmed. Two Lyman break galaxies at $z \gtrsim 7.0$ were recently spectroscopically confirmed by Vanzella et al. (2011), their luminosities fairly consistent with that of the well-known confirmed $z = 6.96$ Iye et al. (2006) Ly α emitter. At present, small number statistics severely affect our ability to draw definite conclusions on the Ly α luminosity function and properties of the IGM. It is therefore essential to expand the sample of high-redshift candidates at epochs when the IGM became metal-enriched and reionized, and thus shed light on the nature of the early universe.

As redshift increases, galaxy sizes and luminosities decrease, and cosmological dimming must also be taken into account. Because of this, detection of galaxies at $z > 7$ can be quite difficult (Ferguson et al. 2004; Bouwens et al. 2006; Capak et al. 2011). Thus it is essential to have a large survey volume in order to detect a sufficient number of high- z objects. This conclusion is bolstered by the biased nature of galaxy formation and the non-uniformity of

large-scale structure at high- z (Steidel et al. 1999; Malhotra et al. 2005; Wang et al. 2005; Ouchi et al. 2005; Tilvi et al. 2009). Presently, most studies searching for high- z galaxies have significant depth but small area (e.g., Bouwens et al. 2010; Oesch et al. 2010) or have small volume but high magnification by virtue of cluster lensing (Richard et al. 2007, 2008; Stark et al. 2007), so all results are affected by cosmic variance. There is a need for surveys which probe both a deep and wide region in order to best constrain global properties of high- z galaxies; the present paper reports on a survey that tries to fill that role.

In this paper, we present the results from a search for Ly α emitting galaxies at $z = 7.7$ in the COSMOS field, utilizing custom-made ultra-narrowband filters which are tuned to avoid the OH sky lines and thus reach extremely low infrared sky backgrounds. The organization of this paper is as follows. In Section 2, we discuss our observations and reduction of the data that we obtained, as well as photometric calibration. In Section 3, we describe our method of candidate Ly α emitter selection and the basic properties of the resulting candidate Ly α emitters. In Section 4, we discuss possible sources of contamination in our samples. In Section 5, we estimate the number of Ly α emitting galaxies that we should expect to find in our survey through the use of a detailed Monte Carlo simulation. In Section 6, we present the Ly α luminosity function derived from our candidates and compare to previously derived Ly α LFs. Finally, in Section 7, we summarize our conclusions. This work shares authors, instrument, and technique with the work of Tilvi et al. (2010), and can thus be viewed as part of a series with that paper. Throughout this work, we assume a standard flat Λ CDM cosmology with $\Omega_m = 0.3$, $\Omega_\Lambda = 0.7$, and $h = 0.71$, where Ω_m , Ω_Λ , and h are the matter density, dark energy density, and Hubble parameter (in units of $100 \text{ km s}^{-1} \text{ Mpc}^{-1}$), respectively. All magnitudes listed are in the AB magnitude system.

2. OBSERVATIONS AND DATA

2.1. Observations with NEWFIRM

Our observations were centered on the Cosmological Evolution Survey (COSMOS) field (RA 10:00:28.6, Dec. +02:12:21.0), taking advantage of the large amount of ancillary data available on this field¹. We used the NOAO Extremely Wide-Field Infrared Mosaic (NEWFIRM) camera on the Mayall 4m telescope at Kitt Peak National Observatory (KPNO) on three different observing runs over the course of two years (2008 February 28 - March 14; 2009 January 29 - February 1; 2009 February 17 - March 2) for a total of roughly 100 hours

¹<http://cosmos.astro.caltech.edu>

over 32 nights. Average seeing over the course of these exposures was $\sim 1.2''$.

The NEWFIRM camera, sensitive to 1-2.4 μm wavelengths, is a wide-field imager consisting of four mosaiced 2048 x 2048 pixel ALADDIN InSb arrays, $0.4'' \text{ pixel}^{-1}$, for a cumulative field of view of $27.6' \times 27.6'$ (cumulative area $\sim 760 \text{ arcmin}^2$). Our observing time was split evenly between two University of Maryland custom-made ultra-narrowband (UNB) filters ($R \sim 1000$) centered at 1.056 and 1.063 μm , with FWHM of 7.4 and 8.1 \AA , respectively. These UNB filters were designed in order to isolate $\text{Ly}\alpha$ emitters at $z \sim 7.7$, while simultaneously avoiding the bright OH lines near these wavelengths (Figure 1 shows UNB filter profiles). The transmitted wavelength varies across the field according to roughly $m\lambda = \mu d \cos \theta$ (here the order, m , index of refraction, μ , and thickness of the filter, d , are constant; θ is the angle of incidence of light onto the detector); the path length increases as one gets further off-axis and the wavelength of transmitted light is correspondingly shorter. This effect is more apparent for a UNB filter in a wide field imager, since the bandpass is narrow and the range of angle of incidence is large (see Figure 1). Atmospheric absorption (primarily due to O_2 and H_2O in the IR) is irrelevant in these bandpasses. Each 1200s exposure science frame was taken using Fowler 8 sampling and we utilized random dithering within a $45''$ box after each exposure.

Additional ancillary data in broadband filters were required for $\text{Ly}\alpha$ candidate selection. We made use of publicly-available data from the COSMOS archive² for this purpose: B , r , and i band data from Subaru and J band data from UKIRT.

2.2. Data Reduction

The reduction of our data was done by the NEWFIRM Science Pipeline (see Dickinson and Valdes 2009; Swaters et al. 2011). Frames with seeing of $> 1.5''$ were rejected outright. The pipeline flagged pixels affected by detector blemishes, saturation, and persistence, and then subtracted the dark current, linearized the data, and applied the dome flat. Image gradients remaining after the flat fielding were subtracted out. The astrometric solution was determined from 2MASS stars in the field; these same stars were also used to determine an initial photometric calibration of the data. In the pipeline, the sky was subtracted in a two-pass approach. First, the sky was subtracted using a running-median window, and then the data were combined by taking the median over all the exposures. This so-called harsh stack was then used to identify and mask sources. The mask was then applied to the original images, and the sky-subtraction was repeated. Cosmic ray hits and other transient

²<http://irsa.ipac.caltech.edu/Missions/cosmos.html>

phenomena were detected by comparing individual images against the first-pass stack, and outliers were flagged.

Starting with these pipeline products, custom IDL4 scripts designed by Krug & Swaters were used to eliminate artifacts such as OH rings and striping due to data readout from the science frames. For OH ring elimination, pixel values were separated into 1000 radial bins across one NEWFIRM chip at a time. Owing to the unevenness of the NEWFIRM chip gaps, the pixel center of the OH ring varied from chip to chip; the ring centers were determined for each chip through a combination of visual inspection and fitting rings to the values at each pixel. Data within the radial bins were then median smoothed, and these smoothed bins were then subtracted from the original image data. Stripe removal was also performed on individual NEWFIRM chips at one time. Each chip was divided into horizontal or vertical strips, depending on data readout direction. Pixels across each strip were summed and averaged, and the original data pixels in each strip were subtracted by the average pixel value in that strip. A comparison of stacks made from frames before and after ring and stripe removal showed that the signal-to-noise ratio (SNR) increased by 1.2 times on average across the frames, with SNR increasing by as much as 4-7 times in regions where the OH rings were strong prior to algorithm implementation. The SNR in the most extreme rings, however (namely those areas as seen in Figure 1 where the OH lines cross the outer edge filters, particularly the strongest OH ring in the 1.063 μm filter), was not quite high enough for candidate detection (see Section 3).

Following removal of artifacts and sky subtraction, the world coordinate system of each individual frame was assigned using the IRAF task *nfwcs*, which matches as many sources as possible to those of the 2MASS point source catalog, searching within a 450" radius. The *mscimage* task was used to reproject all four chips onto a single image with the same pixel grid. Finally, images were combined into two yearly stacks (weighted by seeing) as well as one full data stack for each filter via *imcombine*; these were median combined using noise values from *mscstat* and zeropoint magnitudes as calculated based on the 2MASS catalog during the prior *nfwcs* task. This resulted in two full UNB stacks - one each for the 1.056 and 1.063 μm filters - as well as stacks from year one and year two for each filter (in order to properly check for transients). Broadband data mosaics supplied by the COSMOS team were already reduced.

2.3. Photometric Calibration

Photometric calibration was performed by making use of the 2MASS point source catalog. SExtractor (SE; Bertin & Arnouts (1996)) was run on each NEWFIRM UNB stack

using a magnitude zero point set to zero. The resulting catalogs were matched with the 2MASS point source catalog; in order to avoid saturated sources or objects that are too faint, all stars with 2MASS J band magnitudes (AB) of less than 13.0 or greater than 16.5 were discarded. Plots were made comparing the SE UNB magnitudes with 2MASS J magnitudes in order to determine an appropriate zeropoint. Before SE could be run with the proper magnitude zeropoint, it was necessary to determine a color correction between the 2MASS J magnitude and the NEWFIRM UNB magnitudes, as they do not share the same central wavelength. 2MASS J , H , and K band magnitudes for overlapping stars were converted to flux and used to calculate the flux expected at 1.056 and 1.063 μm , the central wavelengths of the NEWFIRM UNB filters. The difference between 2MASS J flux and extrapolated NEWFIRM UNB flux corresponds to a magnitude difference of $\sim +0.1$ mag in J . This correction was then applied to the previously determined magnitude zeropoint.

2.4. Limiting Magnitude

In order to determine which of our detections can be considered real, we must obtain some estimate of the limiting magnitude of our science frames. We have chosen to define our limiting magnitude as the 50% completeness limit in our frames. To determine this, we inject artificial sources into our frames. These sources are randomly distributed throughout each frame, although care is taken to avoid locations within $4''$ of any existing bright star. Two hundred artificial point sources are generated in each of 0.1 magnitude bins, ranging between 20 and 24 mag for UNB frames, 21 and 25 for J band, and 24 and 28 mag for the broadband optical frames. Once these sources were generated, SE was run and the resultant SE catalog was matched with the catalog of artificial sources to determine a recovery fraction. This procedure was then iterated 25 times for each band. Once all iterations were completed, histograms of recovery fraction of artificial sources were plotted for each band in order to determine the magnitude at which 50% of all artificial sources were detected by SE (Figure 2 for UNB recovery fraction histograms). We define the limiting magnitude for each band as the 50% completeness limit for that filter, as this is the magnitude brighter than which sources can be reliably detected in these fields via our methods. Limiting magnitudes for the two NEWFIRM UNB bands were determined to be 22.4 and 22.5 (AB) for 1.056 μm and 1.063 μm , respectively. Shifts in central wavelength of the UNB filters with distance from the field center were not found to significantly affect these limiting magnitudes. For the broadband data, limiting magnitudes were found to be 27.3, 26.6, 26.3, and 24.0 for B , r , i , and J , respectively.

3. CANDIDATE Ly α EMITTERS

3.1. Selection Criteria

To select potential candidate Ly α emitters, we initially ran SE on the NEWFIRM UNB frames individually, with minimum detection area of 5 pixels and detection threshold of 1.2 sigmas. We then used dual-image mode in SE, which takes the coordinates of objects detected in the NEWFIRM UNB frames but measures fluxes at those coordinates in the UKIRT J band image. Thus we obtained J band fluxes at the exact locations of NEWFIRM UNB targets. For all of our dual-image mode detections, we made use of the SExtractor auto aperture size scaling. We also needed to obtain optical fluxes at those coordinates, so in order to do so, we created a chi-squared image of a combination of B , r , and i band data from Subaru using the program *Swarp* (Bertin et al. 2002). The chi-squared image is created by deriving the distribution of the pixels that are dominated by object flux rather than those dominated by sky noise (Szalay et al. 1999). This is an optimal combination of images which enhances real objects in the resultant frame rather than a simple stack. We then ran SE in dual-image mode on this combined optical image in the same vein as the J images. We also ran dual-image mode on the two NEWFIRM UNB frames together - first using the coordinates for 1.056 μm detections but getting 1.063 μm flux, and vice versa - as any potential candidate Ly α emitter should appear in one of the UNB frames but not both. We likely miss highly extended Ly α blobs with this technique, especially following sky subtraction, but such highly extended sources would be difficult to isolate in any case.

Once the SE catalogs were created, we ran a custom python script to comb through those catalogs and identify potential candidates. There were five main initial criteria that had to be met in order for an object to be considered a candidate (J data refers to the UKIRT band, centered at 1.2 μm and outside the UNB filter range):

1. UNB signal-to-noise ratio (SNR) of at least 5.
2. UNB excess $f_\nu(\text{UNB}) - f_\nu(J)$ of at least 3σ .
3. Flux ratio $f_\nu(\text{UNB}) / f_\nu(J)$ of at least 2.
4. UNB SNR in the other UNB filter of no more than 2 (e.g. if detected in 1.056 μm , must not have a 1.063 μm SNR of more than 2).
5. Optical SNR in the chi-squared broadband image of no more than 2.

These selection criteria have been utilized in lower redshift ($z = 4.5, 5.7$) searches for Ly α emitters and have detected those emitters at a 70-80% success rate after spectroscopic

confirmation, and we are confident that these criteria will translate to higher redshift, as the fundamental physics of the Ly α forest should not change, and similar criteria have been used in a successful spectroscopic search at $z = 6.96$ (see, e.g., Rhoads & Malhotra 2001; Rhoads et al. 2003; Dawson et al. 2004; Iye et al. 2006; Dawson et al. 2007; Wang et al. 2009). These criteria are also the same as those used in the work of Tilvi et al. (2010). The first three criteria are used to isolate emission line sources. The remaining two are used to eliminate as many low-redshift sources as possible; as detailed in Section 1, Ly α emitters should have no flux blueward of their Ly α emission line, and the Ly α line should be narrow enough that it is only detected in one NEWFIRM UNB filter and not both.

Following execution of the selection script, we were left with 65 potential candidates out of 31254 initial detections for the 1.056 μm band, and 110 potential candidates out of 32382 initial detections for the 1.063 μm band. We then matched our target lists to the existing COSMOS source catalogs (obtained from Peter Capak of the COSMOS team; personal communication). All targets which met our selection criteria but which were also in the COSMOS catalog with a measured photometric redshift were set aside (Section 4.1 for further information on these low-redshift interlopers). Once the low- z interlopers were removed, target lists were then narrowed down further through a variety of methods: eliminating all targets on the edges of the chip which lie in or outside the main OH-line ring; eliminating all targets that lie within two arcseconds of the chip gap (5 pixels); eliminating all targets within two arcseconds from a very bright star. Roughly 90% of the initial non-interloper candidates were removed this way. Basic visual inspection was then performed as a sanity check. Our targets were also compared with the yearly stacks for each filter (both via SE and visual inspection) in order to ensure that these targets were not transients (Section 4). As a final sanity check, we did not consider any candidates with magnitudes fainter than the limiting magnitudes for each filter (Section 2.4).

3.2. Results

After all these tests were completed, we were left with a total of 4 candidates brighter than the 50% completeness limit - 3 candidates in 1.056 μm , 1 in 1.063 μm . Three of these candidates lie at the survey line flux limit. The coordinates and basic properties of these four luminous candidates - AB magnitude, line flux, and luminosity - are listed in Table 2. Line flux was calculated from the SExtractor magnitude using:

$$F = 10^{-0.4*(\text{mag}_{\text{AB}}+48.60)} \frac{c}{\lambda^2} W \text{ ergs}^{-1}\text{cm}^{-2}\text{s}^{-1}, \quad (1)$$

where mag_{AB} is the magnitude from the isophotal fit as reported by SExtractor, c is the speed of light, λ is the central wavelength of the given filter, and W is the filter width ($6.95 \times 10^{-4} \mu\text{m}$ for the $1.056 \mu\text{m}$ filter, $7.49 \times 10^{-4} \mu\text{m}$ for 1.063). Whereas we used the SE auto fit for initial dual-image mode detection, we use isophotal fit for flux calculation to avoid losing signal and gaining noise. We can also estimate the star formation rates for these objects, assuming that there is little attenuation of the $\text{Ly}\alpha$ line by the neutral IGM and that the dust content along the line of sight is low. We use the following prescription from Ota et al. (2010), which uses the Kennicutt law (Kennicutt 1998) and assumes case B recombination:

$$\text{SFR}(\text{Ly}\alpha) = 9.1 \times 10^{-43} L(\text{Ly}\alpha) M_{\odot} \text{ yr}^{-1}. \quad (2)$$

Using this calculation, we find that star formation rates for our four $\text{Ly}\alpha$ candidates range from 5 to $7.6 M_{\odot} \text{ yr}^{-1}$. Postage-stamp images of these candidates are shown in Figure 3. Note that each candidate is visible in one particular NEWFIRM UNB stamp but is not visible in the other NEWFIRM UNB stamp. Additionally, no candidate is visible either in the chi-squared broadband optical stamp nor the UKIRT J band stamp. As stated in Section 3, in order to eliminate most foreground galaxies, it is required that none of the candidates are detected in the broadband image; non-detection in the J band image is simply due to the faint continuum of the $\text{Ly}\alpha$ candidates. As can be seen in Figure 3, the PSF is considerably better in the Subaru band stack than in our UNB data. To try to determine whether this could affect our candidate selection, we have attempted a modified aperture correction using a comparison between total SE auto flux in the Subaru field and flux derived from isophotal fits; this correction allows us to account for faint sources in the optical image. Following this correction, we re-ran our selection criteria. Three of our four high- z $\text{Ly}\alpha$ candidates still passed the selection criteria, but candidate #3 failed selection following this aperture correction (optical $\text{SNR} > 2$). We still include candidate #3 in the following analysis but flag it in Table 2 as more uncertain than the other candidates.

3.3. $\text{Ly}\alpha$ Equivalent Widths

As we have a sample of four strong candidate $\text{Ly}\alpha$ emitters, it is worthwhile to compare the equivalent widths (EWs) of their $\text{Ly}\alpha$ emission lines to those already noted in the literature. Several published studies have spectroscopically identified $\text{Ly}\alpha$ emitters with rest-frame equivalent widths of $\text{EW}_{\text{rest}} > 240 \text{\AA}$ at $z = 4.5$ and 5.7 , significantly higher than predicted by theoretical simulations of star-forming galaxies (Malhotra & Rhoads 2002; Shimasaku et al. 2006; Dawson et al. 2007; Gronwall et al. 2007; Ouchi et al. 2008).

The calculation for rest-frame EW for our Ly α emitters makes use of the fluxes measured in both the NEWFIRM UNB filters and the broadband UKIRT J data, as the Ly α line does not appear in the J band (again, the J band data is centered at $1.2\mu\text{m}$, with no overlap with our UNB filters). However, none of our candidates were detected in the J band, and thus we must use the J band limiting magnitude (Section 2.4) to calculate an upper limit on J band flux. In this case, given the limiting magnitude of 24.0 in the UKIRT J band, the upper limit on the J band continuum flux $f_{\lambda,J} = 1.9 \times 10^{-19} \text{ erg s}^{-1} \text{ cm}^{-2} \text{ \AA}^{-1}$. This value is used to calculate a lower limit on the rest-frame Ly α EW for our candidates:

$$\text{EW}_{\text{rest}} = \frac{f_{\text{UNB}}}{f_{\lambda,J}} \times \frac{1}{1+z}, \quad (3)$$

where f_{UNB} is the UNB line flux in $\text{erg s}^{-1} \text{ cm}^{-2}$. This calculation assumes that the Ly α line falls entirely within the transmission profile of our UNB filters. In reality, the UNB filters may not enclose all of the Ly α emission. Moreover, we are using upper limits on the J band fluxes. The EWs measured in this way should thus be viewed as $1\text{-}\sigma$ lower limits. This calculation also assumes an exact redshift of $z = 7.7$.

The resultant lower limits on the rest-frame EW (Ly α) are 7.32, 5.17, 4.89, and 4.84 \AA for candidates 1-4, respectively. Thus our lower limit on EW for our candidates is $\text{EW}_{\text{rest}} \gtrsim 4.8 \text{ \AA}$, much more consistent with theoretical predictions than the numbers quoted above for lower redshift surveys. Our lower limit EW is smaller than that of Hibon et al. (2010) by several angstroms, primarily owing to the difference in bandwidths of UNB filters used by these two surveys. This line width is also larger by $\sim 2 \text{ \AA}$ than the results of the Tilvi et al. (2010) survey, although this difference can be accounted for by the increase in depth of our J band data (limiting magnitude of 24.0 for our data versus 23.5 for their data). As future surveys obtain deeper J band data, we should be able to better constrain the lower limits of Ly α EWs for these emitters.

4. POSSIBLE SAMPLE CONTAMINATION

There are several possible sources of contamination in our sample of candidate Ly α emitters. These include such real sources as foreground emitters, transients, and cool L & T dwarfs, as well as false sources such as detector noise spikes and general false detections. We discuss each class of contaminants below.

4.1. Foreground Emission Line Sources

There are three main species of foreground emission line objects which are most likely to contaminate our sample, as each species should have a strong emission line that falls within our UNB filter window and, assuming faint continuum emission, negligible flux in nearby blue- and redward bands. These species are H α λ 6563 emitters at $z = 0.62$, [O III] λ 5007 emitters at $z = 1.12$, and [O II] λ 3727 emitters at $z = 1.85$. Given the extensive amount of ancillary data available for the COSMOS field, we were able to first check our catalog with the main COSMOS catalog and eliminate any low- z interlopers from our Ly α candidate list, as mentioned in Section 3. A total of 3 interlopers fulfilled the five main Ly α emitter selection criteria (Section 3), all in the 1.063 μ m filter – one brighter than the limiting magnitude of the field – which were removed from the sample of Ly α candidates. These faint objects, however, are not at the exact redshifts listed above: the COSMOS photometric redshifts are $z \sim 1.5 \pm 0.2$ (1σ ; possibly corresponding to redshifted H γ), $z \sim 1.7 \pm 0.2$ (possibly [OII] λ 3727), $z \sim 2.5 \pm 0.2$ (possibly broad Mg II λ 2798), but the errors may be even larger. It is possible that there remain some foreground emission line objects in our Ly α candidate sample that do not have tabulated photometric redshifts. Our survey benefits greatly from the multi-wavelength coverage and accurate photometric redshifts of the COSMOS data catalog; the presence in our sample of interlopers with photo- z s different from the three expected species listed above may imply that surveys in other fields without such comprehensive ancillary data coverage suffer from greater low- z contamination than estimated.

To estimate the number of additional possible emission line source interlopers that could remain among our candidates, we must estimate the minimum equivalent width required for these emission lines to contaminate our sample. We must also use the depth of our UNB image in order to calculate the minimum luminosities of these emission lines. As described in Section 2.4, the limiting magnitude of our 1.056 μ m stack is 22.4, which is equivalent to a 50% completeness limit in flux of 7.4×10^{-18} erg s $^{-1}$ cm $^{-2}$. Given the redshifts of the aforementioned emission lines and using *CosmoCalc*³ to calculate luminosity distances, we find that the minimum luminosities required to detect these emitters are 1.15×10^{40} erg s $^{-1}$, 4.96×10^{40} erg s $^{-1}$, and 1.72×10^{41} erg s $^{-1}$ for H α , [O III], and [O II] respectively. To calculate the necessary minimum equivalent width (observer-frame), we use the prescription from Rhoads & Malhotra (2001):

$$\text{EW}_{\min} \equiv \left[\frac{f_{\text{nb}}}{f_{\text{bb}}} - 1 \right] \Delta\lambda_{\text{nb}} = \left[\frac{5\sigma_{\text{nb}}}{2\sigma_{\text{bb}}} - 1 \right] \Delta\lambda_{\text{nb}}, \quad (4)$$

³<http://www.astro.ucla.edu/~wright/CosmoCalc.html>

where f_{nb} and f_{bb} refer to the flux densities of the UNB and the chi-squared optical image, respectively, σ_{nb} and σ_{bb} refer to the flux measurement uncertainties in the two frames, and $\Delta\lambda_{\text{nb}}$ is the width of the UNB filter. For these calculations, we have simply used the 1.056 μm UNB filter. It is safe to assume that the continuum contribution to the overall flux in the UNB filter is negligible, since the overall width (effective FWHM) of the transmission profile of the 1.056 μm filter is only 9 \AA (6.95 \AA). For our filters, $\sigma_{\text{nb}} = 1.06 \times 10^{-29} \text{ erg cm}^{-2} \text{ s}^{-1} \text{ Hz}^{-1}$ and $\sigma_{\text{bb}} = 2.1 \times 10^{-31} \text{ erg cm}^{-2} \text{ s}^{-1} \text{ Hz}^{-1}$. This results in a minimum equivalent width for the foreground emission line contaminants of $\text{EW}_{\text{min}} \gtrsim 870 \text{\AA}$.

Although the distribution of equivalent widths of these three species of emitters has not been probed at the high redshifts of our observations, we can scale the published results under the assumption that the luminosity functions of these species have not evolved significantly between the relevant redshifts. One particular recent study has probed emission line sources of $\text{H}\alpha$ at $z = 0.27$, $[\text{O III}]$ at $z = 0.51$, and $[\text{O II}]$ at $z = 1.0$ in the GOODS-South field (Straughn et al. 2009). The minimum EW calculated above was scaled appropriately in each instance to the EW one would expect at the redshifts probed by the Straughn et al. (2009) survey. Using that value and the required minimum luminosity listed above, we determined how many emission line objects we should expect in our field, after scaling appropriately by the ratio of survey volumes. We find that we expect less than one additional interloper for each species (0.1 each for $\text{H}\alpha$ and $[\text{O II}]$, 0.3 for $[\text{O III}]$). If we relax the minimum equivalent width criterion to 500 \AA prior to scaling EWs to what would be expected at $z = 7.7$, the expectation increases to 1 additional interloper each for $\text{H}\alpha$ and $[\text{O II}]$, and 2 additional interlopers for $[\text{O III}]$.

4.2. Other Possible Contaminants

The utilization of individual yearly stacks, as well as nightly stacks, which were produced by the data reduction pipeline, allowed us to eliminate both possible detections due to noise spikes as well as real sources such as transient objects. We required during our candidate selection process that potential candidate $\text{Ly}\alpha$ emitters be detected in all stacks as well as the overall stack, though the detection requirements for individual nightly/yearly stacks were less stringent. This eliminates contamination by noise spikes from the detector, as such noise spikes should not be present at the same coordinates across multiple nights over a span of years. Transients will also be eliminated by this yearly stack check, as supernovae should only be visible for a few weeks, not years. We were able to eliminate upward of twenty contaminants via this requirement.

In order to determine whether any false detections were contaminating our candidate list, we checked to see whether taking the negative of our UNB stacks would result in a detection. We used IRAF to multiply each UNB stack by -1 and then ran SExtractor on the resultant negative images. The SE negative stack catalogs were then run through the exact same selection process as the positive stack catalogs, but no candidates were identified this way. We are thus confident that the probability of false detections contaminating our Ly α sample is insignificant.

The final source of potential contaminants consists of cool stars - namely, L and T dwarfs - passing our selection process. We use previously observed relationships between spectral type and absolute magnitude (Tinney et al. 2003) to determine in what J band magnitude range L and T dwarfs fall, and then we use our calculated J band limiting magnitude to determine distance ranges at which we should be able to see these objects. We find that L dwarfs could be detected between roughly 550 and 1700 pc, and T dwarfs could be detected between roughly 200 and 750 pc. These L and T dwarfs are most likely found within a Galactic disk scale height of 350 pc, however (Ryan et al. 2005) – the number density drops significantly above the scale height of the disk – and thus knowing that these dwarfs typically have a volume density of no more than $\sim 3 \times 10^{-3} \text{ pc}^{-3}$, we thus can conclude that we should expect at most one L or T dwarf in our survey. If we then take our selection criteria into account, we can determine if any L and T dwarfs would satisfy our narrowband excess criterion. Tilvi et al. (2010) used existing observed spectra of L and T dwarfs and a calculation of expected flux through our NEWFIRM filters. They determined that the flux which would be transmitted through the NEWFIRM UNB filters, in comparison to that which would be transmitted through the NEWFIRM J filter, would not be sufficient to pass our narrowband excess criterion. Thus, we should expect that no L nor T dwarfs would pass our selection criteria and contaminate our sample.

5. MONTE CARLO SIMULATIONS

As discussed in Section 4, we do not expect all of our four candidate Ly α emitters to be real, as it is possible that further low- z emission line source interlopers may pass our selection criteria. In order to determine how many of our Ly α candidates we should expect to be real, we run Monte Carlo statistical simulations using previously known Ly α luminosity functions at lower redshift. In this work, we make use of the Kashikawa et al. (2006) Ly α luminosity function at $z = 6.5$ and assume that there has been no significant evolution between $z = 6.5$ and $z = 7.7$. These simulations also make use of the fact that the NEWFIRM UNB filter transmission curves may not encompass the full width of the expected Ly α emission lines

in these objects, and thus our measurements may in fact be underestimating the Ly α line flux produced by our Ly α candidates. The transmission curves of our two UNB filters were obtained from the NEWFIRM website^{4,5}.

To begin our Monte Carlo simulations, we utilized the aforementioned Kashikawa et al. (2006) luminosity function to generate one million random galaxies. These galaxies were distributed with both a random Ly α luminosity in the range of 10^{42} erg s $^{-1}$ to 1.5×10^{43} erg s $^{-1}$, as well as a random redshift in the range probed by our filters. In the case of the 1.056 μm band, this range is $7.66 < z < 7.71$; for the 1.063 μm band, this range is $7.72 < z < 7.76$; we chose these ranges to correspond to the full width of the transmission profile at which the transmission falls to 5%.

From these luminosities and redshifts, we were then able to assign a flux to each of our randomly generated galaxies. We made use of an asymmetric Ly α line flux profile based on spectra of $z = 5.7$ Ly α emitters taken by Rhoads et al. (2003). We were able to then use the detailed NEWFIRM UNB filter transmission curve profiles to derive the flux that would pass through the filter via a convolution of filter profile and line flux according to $f_{\text{trans}} = \int f_{\lambda} T_{\lambda} d\lambda$, where T_{λ} is the NEWFIRM UNB filter transmission curve and f_{λ} is the flux density of the emission line based on the Rhoads et al. (2003) spectra. This takes the likely underestimation of Ly α line flux into account. Following this, we were able to convert the convolved line flux into a magnitude by the use of the formula:

$$\text{mag}_{\text{AB}} = -2.5 \log_{10} \left(\frac{f_{\text{trans}}}{f_0} \right), \quad (5)$$

where

$$f_0 = \frac{3.6 \text{kJy} \times c}{(1.06 \mu\text{m})^2} \times \int T_{\lambda} d\lambda \text{ ergs}^{-1} \text{cm}^{-2}, \quad (6)$$

and c is the speed of light. In order to ensure that all instrumental effects were taken into account, the last step in this process was to incorporate the detection fraction at each magnitude bin (Section 2.4; Figure 2). This detection fraction was multiplied by the number of galaxies in each magnitude bin before we converted those magnitudes to Ly α luminosities. The number of detected galaxies in each Ly α luminosity bin was then used to estimate how many Ly α emitters we should expect from our survey.

⁴<http://www.noao.edu/ets/newfirm/documents/1056%20nm%20data%20pack.xls>

⁵<http://www.noao.edu/ets/newfirm/documents/1063%20nm%20data%20pack.xls>

This Monte Carlo simulation was run for each individual NEWFIRM UNB filter and then iterated 10 times for each filter. We then averaged the results of those ten iterations, and the expected number of sources per filter at each magnitude bin is shown in Figure 4. Looking at the limiting magnitudes for each filter and integrating out to that point, we find that we expect ~ 1 source per filter to be a true $z = 7.7$ Ly α emitter. This result should be viewed with some caution, however, as we have assumed that the Ly α luminosity function does not undergo significant evolution between redshifts of 6.5 and 7.7, and that the emission line profiles of all Ly α emitters at $z = 7.7$ are the same as that of a Ly α emission line profile at $z = 5.7$. Moreover, this simulation makes use of the Kashikawa et al. (2006) luminosity function, which is based upon detections in only one field, the Subaru Deep Field. We expect that there will be field-to-field variations among Ly α emitters, and thus the expected number of sources may be different for the COSMOS field. Various methods can be taken to estimate the cosmic variance between fields of these Ly α emitters; for large survey volumes ($\sim 2 \times 10^5$ Mpc 3), Tilvi et al. (2009) estimated this variance to be $\gtrsim 30\%$. We can also utilize the method of Trenti & Stiavelli (2008) to calculate the cosmic variance expected assuming 2 intrinsic Ly α sources as reported by our Monte Carlo simulations. Using the redshift interval of 0.1 for our two filters and a Press-Schechter bias, the Trenti & Stiavelli cosmic variance calculator⁶ returns an expected cosmic variance of $\sim 58\%$ (this number drops by $\sim 10\%$ with Sheth-Tormen bias). In addition to cosmic variance, we note here that the most recent $z=5.7$ and 6.5 Ly α LF results (Hu et al. 2010; Ouchi et al. 2010; Kashikawa et al. 2011) indicate that the predictions for the number densities of $z=7.7$ emitters based on the results of Kashikawa et al. (2006) may be up to a factor of 3 too large. The uncertainty that remains in the lower- z Ly α LFs, taken in concert with the significant role that cosmic variance can play, requires the Monte Carlo simulations to be viewed with caution rather than interpreted at face value.

6. $z = 7.7$ Ly α LUMINOSITY FUNCTION

The primary goal of this work is to constrain the observed luminosity function (LF) of Ly α emitters at $z = 7.7$. As described in the Introduction, our survey has the advantage of being both wide and deep, leading to our volume and limiting flux being better than or comparable to most other surveys at this redshift or higher (Table 1). To construct our $z = 7.7$ Ly α LF, we have used our four targets, which have Ly α line fluxes of 12.1, 8.6, 8.1, and 8.0×10^{-18} erg s $^{-1}$ cm $^{-2}$, all higher than our survey’s limiting flux of 8×10^{-18} erg s $^{-1}$ cm $^{-2}$. Using our survey volume of $\sim 1.4 \times 10^4$ Mpc 3 per filter, we have constructed a

⁶<http://casa.colorado.edu/~trenti/CosmicVariance.html>

cumulative Ly α LF which is shown in Figure 5. In order to calculate the errors, we have used Poissonian statistics with Bayesian likelihood (where the likelihood is equivalent to the probability), assuming each target is in a separate luminosity bin. The assumption in this error model is that the luminosity distribution is uncorrelated - one galaxy having a certain luminosity has no effect on the luminosity of another - and thus it is safe to divide our luminosity bins this finely. As we have a prior probability distribution that is uniform in the expected number m (from Poisson), then the lower and upper limits on our errors are both finite. We have plotted our LF along with the results of several other major surveys. Two of these, Tilvi et al. (2010) and Hibon et al. (2010), focus on the same redshift as our work but have made use of alternate fields (CETUS and CFHT-LS D1, respectively) and thus cosmic variance may come into play. Neither survey has published spectroscopic confirmation at this time, although Clément et al. (2011) note that VLT spectroscopy failed to detect Ly α emission from the five most luminous Hibon et al. (2010) candidates, a result which will be published soon; we plot the Clément et al. (2011) upper limits for $z = 7.7$ Ly α LFs as well. We also plot the spectroscopically confirmed Iye et al. (2006) $z = 6.96$ Ly α emitter. In addition to individual data points, we also plot three curves from previous, slightly lower redshift surveys, which are based on best-fit functions to spectroscopically confirmed data. These include the Ouchi et al. (2008) $z = 5.7$ LF, as well as the well-cited Kashikawa et al. (2006) $z = 6.5$ LF data. We have also included a new data set, the $z = 6.6$ LF from Ouchi et al. (2010), which samples a different field from the Kashikawa $z = 6.5$ LF but agrees well with that data set.

Our data points agree quite well with the findings of Tilvi et al. (2010), despite our surveys probing different fields, but only the most luminous target matches with the Clément et al. (2011) upper limits for $z = 7.7$ within the error; our data points also may seem inconsistent with recent Lyman break surveys (e.g., Pentericci et al. 2011; Schenker et al. 2011). Assuming that all four of our data points are real Ly α emitters at $z = 7.7$, we find good agreement with the $z = 5.7$ Ouchi et al. (2008) function, yet our fainter luminosity objects do not agree with the $z = 6.5$ LF (Kashikawa et al. 2006) nor the $z = 6.6$ LF (Ouchi et al. 2010). This could imply moderate evolution between $z = 7.7$ and $z = 6.6$, yet it is interesting that in such a case, the LFs at $z = 7.7$ and $z = 5.7$ would be in agreement. If we instead take the more conservative approach indicated by our Monte Carlo simulation results and assume only the two most luminous of our targets to be real Ly α emitters, then our results are consistent within error with both the $z = 5.7$ Ouchi et al. (2008) function and the $z = 6.5$ Kashikawa et al. (2006) function. Given that it is more probable statistically that only these two candidates are real, we must take this case as the more likely outcome until we have the ability to spectroscopically verify our sources. Thus, given the agreement of our two most luminous emitters with the LFs at both lower redshifts, there is no conclusive

evidence for evolution of the Ly α LF over the redshift range $5.7 < z < 7.7$.

7. SUMMARY

We have utilized two custom-made UNB filters, at wavelengths 1.056 and 1.063 μm (FWHM 7.4 and 8.1 \AA , respectively) on the NEWFIRM camera at the KPNO 4m Mayall telescope to perform a deep and wide search for $z = 7.7$ Ly α emitters in the COSMOS field. Our study comprised a co-moving volume of $2.8 \times 10^4 \text{ Mpc}^3$ (survey area $\sim 760 \text{ arcmin}^2$) and probed down to a limiting flux of $\sim 8 \times 10^{-18} \text{ erg s}^{-1} \text{ cm}^{-2}$ (50% completeness limit), which is comparable to or better than previous Ly α searches at similar redshifts.

We used a very detailed selection procedure, making use of five different quantitative parameters as well as qualitative methods to ensure narrow-line detection and elimination of contaminants (including 3 low- z interlopers already known in the COSMOS catalog). We were left with a total of four candidates (three detected in the 1.056 μm filter, one in the 1.063 μm filter), each detected at 5 sigmas or higher, down to line fluxes of $8 \times 10^{-18} \text{ erg s}^{-1} \text{ cm}^{-2}$. Detailed Monte Carlo simulations would suggest that up to two of these candidates are real. If we assume only two real candidates, comparison of the resultant Ly α LF to the $z = 5.7$ Ouchi et al. (2008) and $z = 6.5$ Kashikawa et al. (2006) Ly α LFs would indicate that there has been no significant evolution of the Ly α LF between $5.7 < z < 7.7$. This result is consistent with the findings of Tilvi et al. (2010) – that work used the same instrument, equivalent field of view, reached similar flux limits, but was half the volume of our work, owing to our extra filter.

To pin down the neutral hydrogen fraction at $z = 7.7$ and thus the stage of the reionization process at that epoch, we will need more detailed Ly α LFs in order to accurately determine the characteristic luminosity, L^* , of these objects. This will require a) spectroscopic confirmations of these candidate high-redshift Ly α emitters, and b) surveys encompassing more fields, as cosmic variance is likely to affect the number of emitters found in each region. The success of previous narrowband surveys at identifying Ly α emitters at lower redshift and the robustness of our current set of candidates mean that the future of such high- z studies is quite promising. It is also encouraging to note that our results match well with surveys in different fields. The pursuit of surveys such as these, along with the advances that should be brought to the field by JWST and other new instruments, should provide a bright future for the study of the Dark Ages.

H.B.K. and S.V. were supported by the NSF through contracts AST 0606932 and

1009583. H.B.K. would like to acknowledge M. Coleman Miller for helpful discussion of statistics and Bayesian error calculation, and is very grateful to Peter Capak for assistance with the COSMOS data catalog and discussion of COSMOS PSFs and aperture correction methods. Monte Carlo simulations were performed using the University of Maryland’s Yorp computing cluster. The observations reported here were obtained at the Kitt Peak National Observatory, National Optical Astronomy Observatory, which is operated by the Association of Universities for Research in Astronomy (AURA), Inc., under cooperative agreement with the National Science Foundation.

REFERENCES

- Bahcall, J. N., & Salpeter, E. E. 1965, *ApJ*, 142, 1677
- Bertin, E., & Arnouts, S. 1996, *A&AS*, 117, 393
- Bertin, E., Mellier, Y., Radovich, M., Missonnier, G., Didelon, P., & Morin, B. 2002, *Astronomical Data Analysis Software and Systems XI*, 281, 228
- Bouwens, R. J., Illingworth, G. D., Blakeslee, J. P., & Franx, M. 2006, *ApJ*, 653, 53
- Bouwens, R. J., et al. 2010, *ApJ*, 725, 1587
- Capak, P., et al. 2011, *ApJ*, 730, 68
- Clément, B., et al. 2011, arXiv:1105.4235
- Cowie, L. L., & Hu, E. M. 1998, *AJ*, 115, 1319
- Cuby, J.-G., Hibon, P., Lidman, C., Le Fèvre, O., Gilmozzi, R., Moorwood, A., & van der Werf, P. 2007, *A&A*, 461, 911
- Curtis-Lake, E., et al. arXiv:1110.1722
- Dawson, S., et al. 2004, *ApJ*, 617, 707
- Dawson, S., Rhoads, J. E., Malhotra, S., Stern, D., Wang, J., Dey, A., Spinrad, H., & Jannuzi, B. T. 2007, *ApJ*, 671, 1227
- Dickinson, M., & Valdes, F. A. 2009, *Guide to NEWFIRM Data Reduction with IRAF*, NOAO SDM PL017
- Ferguson, H. C., et al. 2004, *ApJ*, 600, L107
- Finkelstein, S. L., Rhoads, J. E., Malhotra, S., & Grogin, N. 2009, *ApJ*, 691, 465
- Fontana, A., et al. 2010, *ApJ*, 725, L205
- Fynbo, J. U., Möller, P., & Thomsen, B. 2001, *A&A*, 374, 443
- Gronwall, C., et al. 2007, *ApJ*, 667, 79
- Gunn, J. E., & Peterson, B. A. 1965, *ApJ*, 142, 1633
- Haiman, Z. 2002, *ApJ*, 576, L1

- Hibon, P., et al. 2010, *A&A*, 515, A97
- Hu, E. M., McMahan, R. G., & Cowie, L. L. 1999, *ApJ*, 522, L9
- Hu, E. M., Cowie, L. L., McMahan, R. G., Capak, P., Iwamuro, F., Kneib, J.-P., Maihara, T., & Motohara, K. 2002, *ApJ*, 568, L75
- Hu, E. M., Cowie, L. L., Capak, P., McMahan, R. G., Hayashino, T., & Komiyama, Y. 2004, *AJ*, 127, 563
- Hu, E. M., Cowie, L. L., Barger, A. J., et al. 2010, *ApJ*, 725, 394
- Iye, M., et al. 2006, *Nature*, 443, 186
- Kashikawa, N., et al. 2006, *ApJ*, 648, 7
- Kashikawa, N., Shimasaku, K., Matsuda, Y., et al. 2011, *ApJ*, 734, 119
- Kennicutt, R. C., Jr. 1998, *ARA&A*, 36, 189
- Komatsu, E., et al. 2011, *ApJS*, 192, 18
- Lynds, R. 1971, *ApJ*, 164, L73
- Malhotra, S., & Rhoads, J. E. 2002, *ApJ*, 565, L71
- Malhotra, S., & Rhoads, J. E. 2004, *ApJ*, 617, L5
- Malhotra, S., et al. 2005, *ApJ*, 626, 666
- Miralda-Escudé, J., Cen, R., Ostriker, J. P., & Rauch, M. 1996, *ApJ*, 471, 582
- Nilsson, K. K., Orsi, A., Lacey, C. G., Baugh, C. M., & Thommes, E. 2007, *A&A*, 474, 385
- Oesch, P. A., et al. 2010, *ApJ*, 709, L21
- Ono, Y., et al. 2011, arXiv:1107.3159
- Ouchi, M., et al. 2001, *ApJ*, 558, L83
- Ouchi, M., et al. 2003, *ApJ*, 582, 60
- Ouchi, M., et al. 2005, *ApJ*, 635, L117
- Ouchi, M., et al. 2008, *ApJS*, 176, 301
- Ouchi, M., et al. 2010, *ApJ*, 723, 869

- Ota, K., et al. 2008, *ApJ*, 677, 12
- Ota, K., et al. 2010, *ApJ*, 722, 803
- Parkes, I. M., Collins, C. A., & Joseph, R. D. 1994, *MNRAS*, 266, 983
- Pentericci, L., et al. 2011, arXiv:1107.1376
- Rees, M. J. 1986, *MNRAS*, 218, 25P
- Rhoads, J. E., & Malhotra, S. 2001, *ApJ*, 563, L5
- Rhoads, J. E., Malhotra, S., Dey, A., Stern, D., Spinrad, H., & Jannuzi, B. T. 2000, *ApJ*, 545, L85
- Rhoads, J. E., et al. 2003, *AJ*, 125, 1006
- Rhoads, J. E., et al. 2004, *ApJ*, 611, 59
- Richard, J., et al. 2007, *ApJ*, 662, 781
- Richard, J., Stark, D. P., Ellis, R. S., George, M. R., Egami, E., Kneib, J.-P., & Smith, G. P. 2008, *ApJ*, 685, 705
- Rousselot, P., Lidman, C., Cuby, J.-G., Moreels, G., & Monnet, G. 2000, *A&A*, 354, 1134
- Ryan, R. E., Jr., Hathi, N. P., Cohen, S. H., & Windhorst, R. A. 2005, *ApJ*, 631, L159
- Ryan-Weber, E. V., Pettini, M., & Madau, P. 2006, *MNRAS*, 371, L78
- Santos, M. R. 2004, *MNRAS*, 349, 1137
- Schaye, J. 2001, *ApJ*, 559, 507
- Schenker, M. A., Stark, D. P., Ellis, R. S., Robertson, B. E., Dunlop, J. S., McLure, R. J., Kneib, J. -, & Richard, J. 2011, arXiv:1107.1261
- Shimasaku, K., et al. 2006, *PASJ*, 58, 313
- Simcoe, R. A., et al. 2011, arXiv:1104.4117
- Sobral, D., et al. 2009, *MNRAS*, 398, L68
- Stark, D. P., Ellis, R. S., Richard, J., Kneib, J.-P., Smith, G. P., & Santos, M. R. 2007, *ApJ*, 663, 10

- Steidel, C. C., Adelberger, K. L., Giavalisco, M., Dickinson, M., & Pettini, M. 1999, *ApJ*, 519, 1
- Straughn, A. N., et al. 2009, *AJ*, 138, 1022
- Swaters, R. A., Valdes, F., Dickinson, M. E. 2011, *Guide to NEWFIRM Data Reduction*, NOAO SDM, in preparation
- Szalay, A. S., Connolly, A. J., & Szokoly, G. P. 1999, *AJ*, 117, 68
- Taniguchi, Y., et al. 2005, *PASJ*, 57, 165
- Tilvi, V., Malhotra, S., Rhoads, J. E., Scannapieco, E., Thacker, R. J., Iliev, I. T., & Mellema, G. 2009, *ApJ*, 704, 724
- Tilvi, V., et al. 2010, *ApJ*, 721, 1853
- Tinney, C. G., Burgasser, A. J., & Kirkpatrick, J. D. 2003, *AJ*, 126, 975
- Trenti, M., & Stiavelli, M. 2008, *ApJ*, 676, 767
- Vanzella, E., Pentericci, L., Fontana, A., et al. 2011, *ApJ*, 730, L35
- Wang, J. X., Malhotra, S., & Rhoads, J. E. 2005, *ApJ*, 622, L77
- Wang, J.-X., Malhotra, S., Rhoads, J. E., Zhang, H.-T., & Finkelstein, S. L. 2009, *ApJ*, 706, 762
- Willis, J. P., Courbin, F., Kneib, J.-P., & Minniti, D. 2008, *MNRAS*, 384, 1039

Table 1. Comparison to previous high- z Ly α searches

z (1)	Survey Vol. (Mpc ³) (2)	Detec. Limits (erg s ⁻¹ cm ⁻²) (3)	# of LAE Detec. (4)	Refs (5)
7.7	6.3×10^4	8.3×10^{-18}	7	Hibon+ 2010
7.7	1.4×10^4	7×10^{-18}	4	Tilvi+ 2010
7.7	2.8×10^4	8×10^{-18}	4	This work
8-10	35	2×10^{-17}	6	Stark+2007
8.8	6.3×10^4	1.3×10^{-17}	0	Cuby+2007
8.96	1.12×10^6	6×10^{-17}	0	Sobral+2009

Note. — Col.(1): Ly α redshift probed. Col.(2): Survey volume. The volume of our study is 2x deeper than Tilvi et al. 2010 owing to our use of a second filter for candidate selection (each filter probes a volume of 1.4×10^4 Mpc³). Col.(3): Survey flux detection limit. Col.(4): Number of candidate Ly α emitters detected. Col.(5): Survey reference.

Table 2. Properties of four candidate Ly α emitters.

Cand. # (1)	RA (2)	Dec (3)	Mag _{AB} (4)	Line Flux (erg s ⁻¹ cm ⁻²) (5)	L _{Lyα} (erg s ⁻¹) (6)	EW _{Lyα} (Å) (7)
1	10:00:46.94	+02:08:48.84	21.87	1.21×10^{-17}	8.34×10^{42}	7.32
2	10:00:20.52	+02:18:50.04	22.25	8.55×10^{-18}	5.90×10^{42}	5.17
3 ^(a)	09:59:56.21	+02:10:09.84	22.31	8.09×10^{-18}	5.58×10^{42}	4.89
4	10:00:48.79	+02:09:21.24	22.39	8.00×10^{-18}	5.52×10^{42}	4.84

Note. — (a) Candidate #3 fails the optical selection criterion following an aperture correction of the Subaru data; it is thus considered more uncertain than the others. Col.(2): RA in J2000. Col.(3): Dec in J2000. Col.(4): AB magnitude, calculated using isophotal flux in SExtractor. Col.(5): Line flux, in the 1.056 μ m band for candidates 1-3 and in the 1.063 μ m band for candidate 4. Col.(6): Ly α luminosity, calculated assuming a redshift of $z=7.7$. Col.(7): Lower limit rest-frame equivalent width of Ly α emission, calculated as described in Section 3.3 equivalent widths.

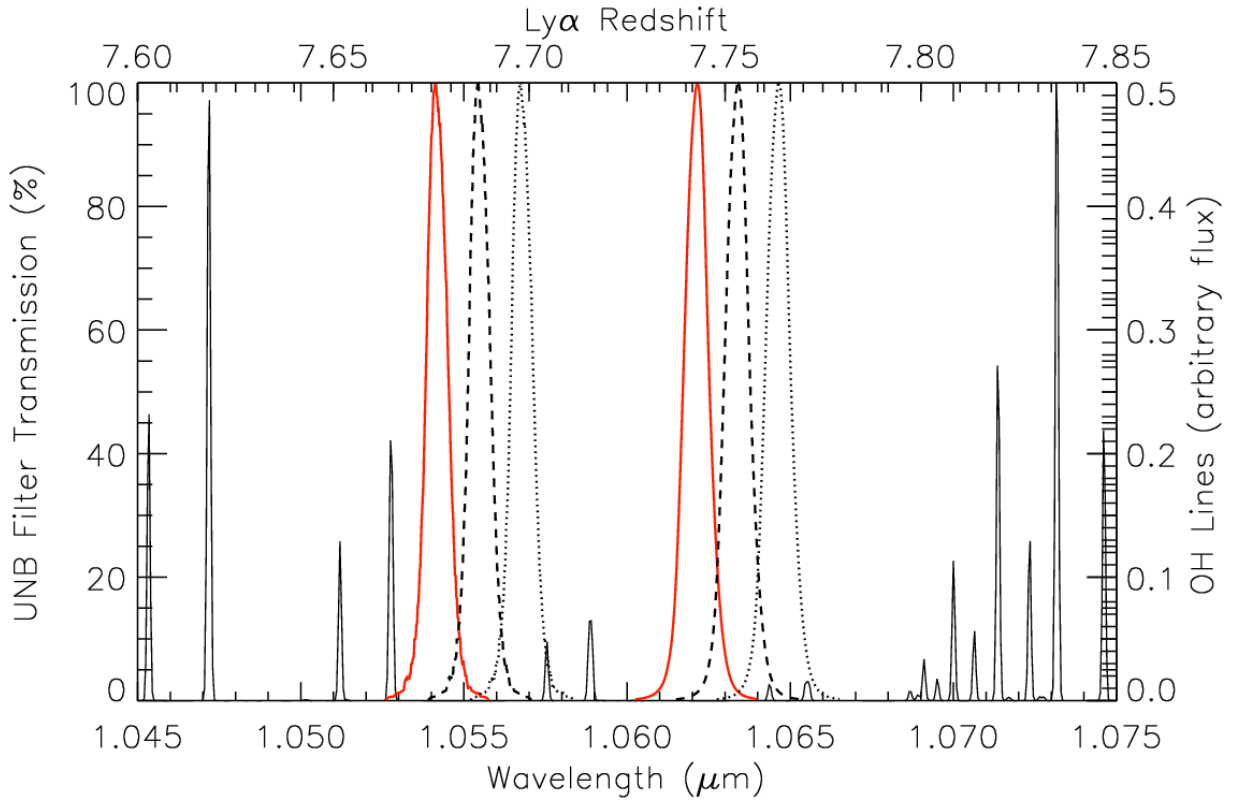


Fig. 1.— NEWFIRM ultra-narrowband filter profiles, centered at 1.056 and 1.063 μm . The solid red, dashed, and dotted lines show the range of profile from center (solid red) to $\sim 40\%$ (dashed) and 80% center-to-corner distance (dotted) of the field of view. The Rousselot et al. (2000) OH sky spectrum is also plotted.

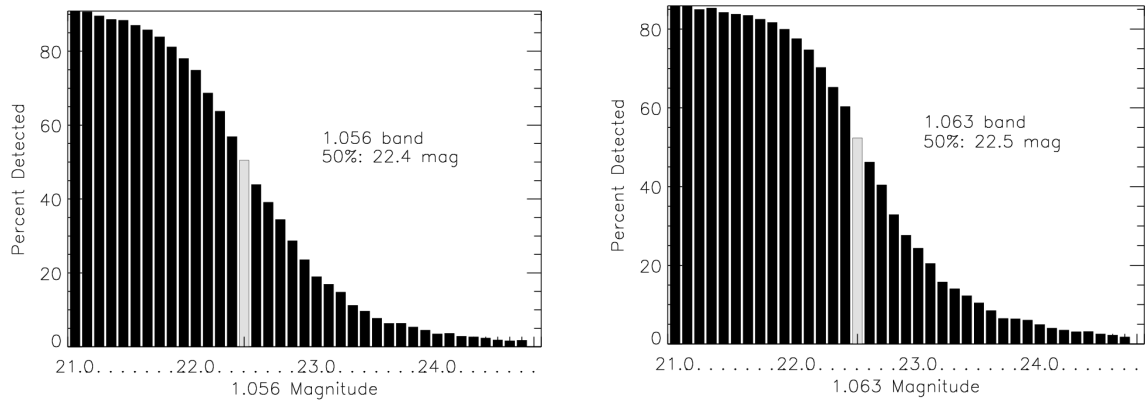


Fig. 2.— SExtractor detection percentages for randomly generated false sources in 0.1 magnitude bins in a given UNB band. The light gray bar marks 50% completeness. That value is used as the limiting magnitude (AB) for our survey. Our 1.063 μm band data is 0.1 mag deeper than our 1.056 μm band data.

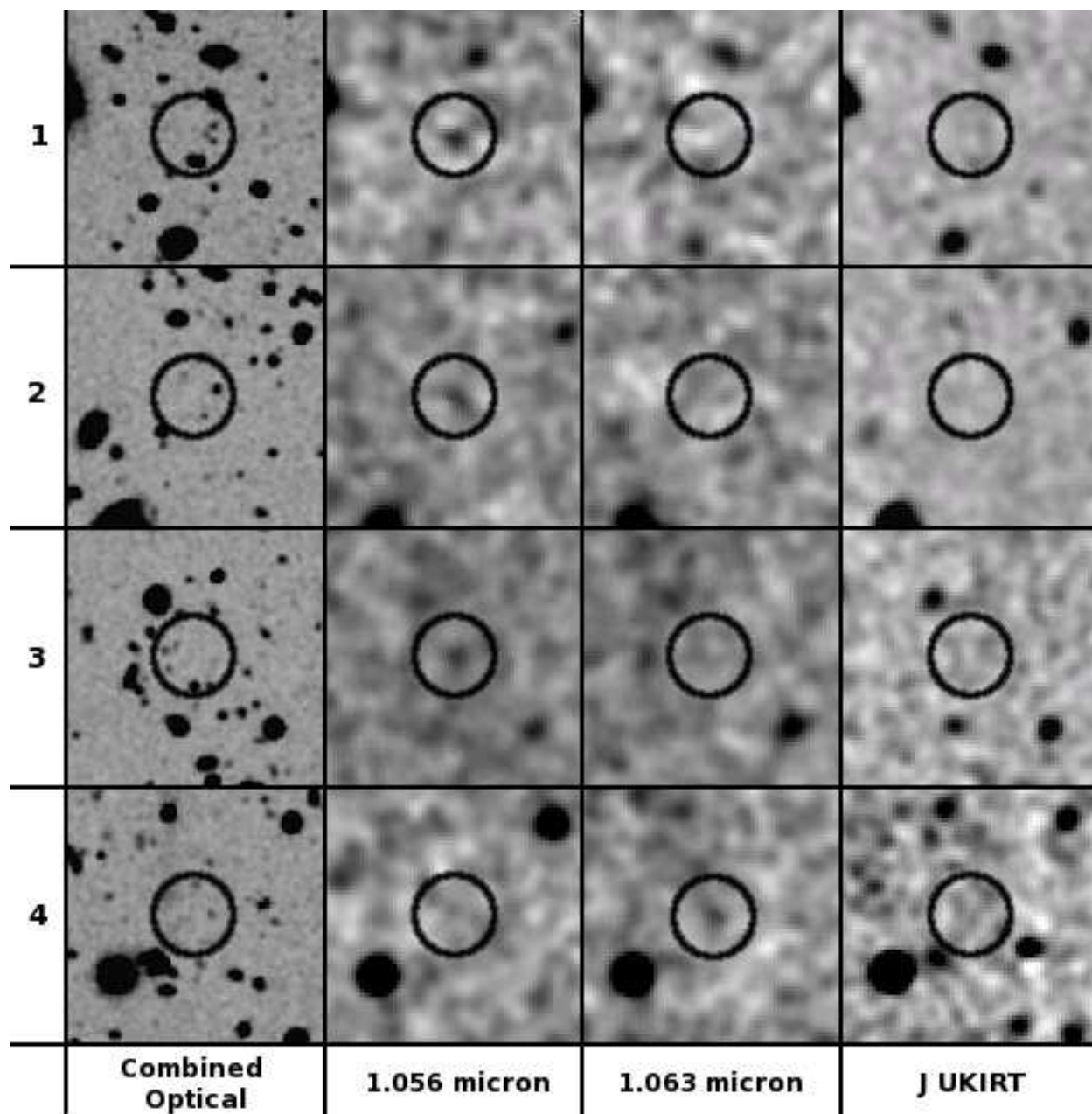


Fig. 3.— Image cutouts for our four $\text{Ly}\alpha$ emitter candidates. UNB cutout images have been Gaussian smoothed according to the average seeing of the 1.056 and 1.063 μm data. Cutouts are $50''$ on each side, and the circles are $16''$ in diameter (corresponding to ~ 400 kpc at $z = 7.7$). Each row represents one candidate. The optical column shows a weighted chi-squared combination of B , r , and i band images from Subaru. The middle two columns show our UNB NEWFIRM data. The J band column represents data from UKIRT. Candidates #1-3 are detected in 1.056 μm but not in any other band; candidate #4 is only detected in 1.063 μm . All other objects present only in one UNB band are either transients (detected in only one yearly UNB stack) or fail to meet the $\text{Ly}\alpha$ selection criteria.

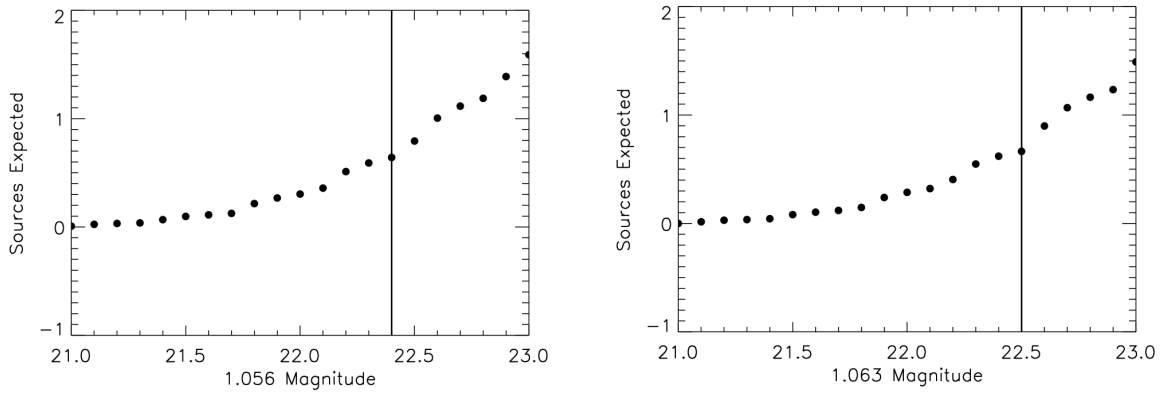


Fig. 4.— Average results of the ten Monte Carlo simulation iterations, showing the number of Ly α emitter sources we should expect at each magnitude bin. Integrating out to our limiting magnitudes for each field (Section 2.4), indicated by the vertical line, we expect roughly 1 source per filter to be a real $z = 7.7$ Ly α emitter if there is no evolution in the luminosity function between $z = 6.5$ and $z = 7.7$.

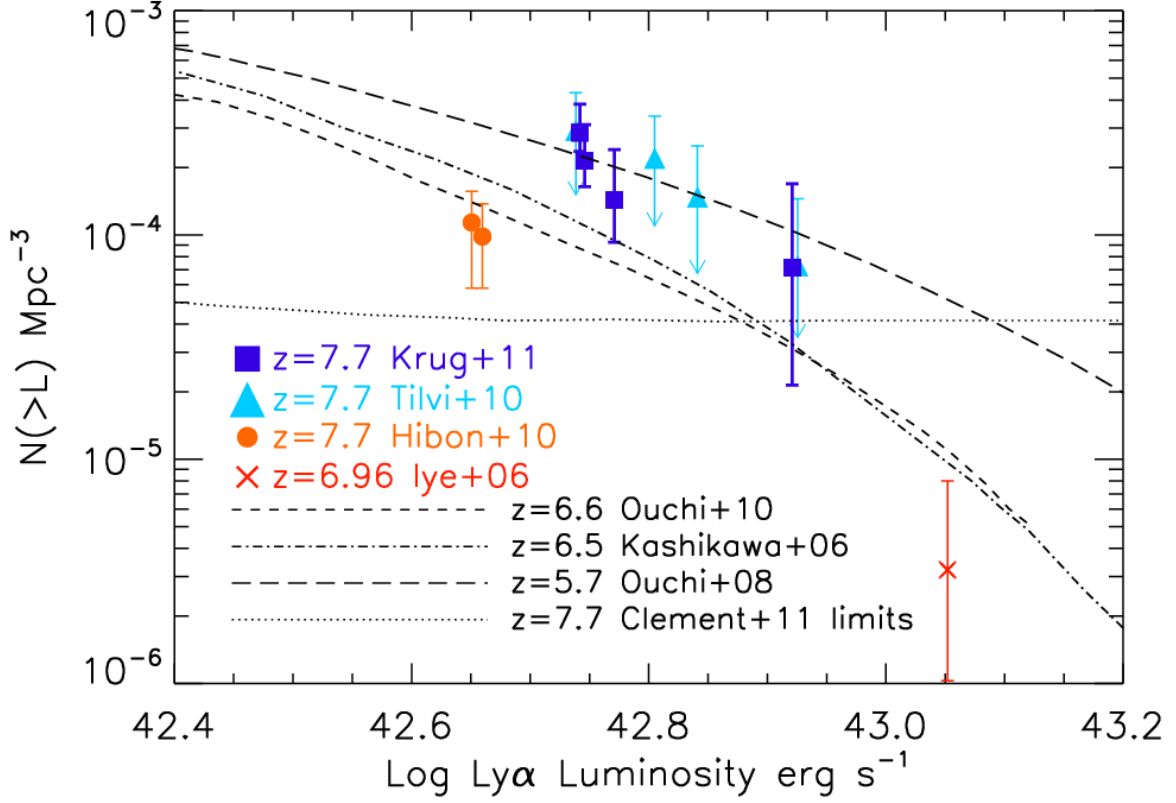


Fig. 5.— Ly α luminosity function compiled from data from this work (dark blue squares) and those previously published. Errors are calculated using Poissonian statistics with Bayesian likelihood. The light blue triangles (Tilvi et al. 2010) and orange circles (Hibon et al. 2010) represent candidates at $z=7.7$ that have not been spectroscopically confirmed. Recent follow-up spectroscopy by Clément et al. (2011) did not detect Ly α emission from the five most luminous candidates of Hibon et al. (2010), so we have excluded these objects from the present figure. The black dotted curve represents upper limits on the $z=7.7$ luminosity function from Clément et al. (2011). The red X (Iye et al. 2006) represents a spectroscopically confirmed $z=6.96$ Ly α emitter. The three black dashed and dashed-dotted curves represent best fit luminosity functions to spectroscopically confirmed Ly α emitters at redshifts $z=5.7$ - 6.6 . Note that our Ly α luminosity function agrees well with that of Tilvi et al. (2011). Our two most luminous candidates are consistent within the error with either the $z=5.7$ or $z=6.5$ luminosity function, and thus we do not see any evidence for significant evolution of the Ly α luminosity function or neutral hydrogen fraction of the IGM between $z=5.7$ and $z=7.7$.